THE ASTROPHYSICAL JOURNAL, 258:260–269, 1982 July 1

HYDRODYNAMICS OF X-RAY INDUCED STELLAR WINDS

RICHARD A. LONDON
Harvard-Smithsonian Center for Astrophysics

AND

BRIAN P. FLANNERY
Corporate Research Science Laboratories, Exxon Research and Engineering Company
Received 1981 July 10; accepted 1982 January 21

ABSTRACT

We present new theoretical models for X-ray induced stellar winds in binary systems. We numerically solve the hydrodynamic equations in one dimension, utilizing a simplified model of the physics of an X-ray heated plasma. The character of the solutions depends on three dimensionless parameters: (1) the ratio of the X-ray spectral temperature to the photospheric temperature; (2) the ratio of the X-ray temperature to a temperature characterizing the escape energy from the stellar surface; and (3) the ratio of the flow time to the heating time. Holding the first parameter fixed at a high value (= 100), we explore the complete range of solutions produced by variations in the other two parameters.

The primary results of the calculations are the temperature and density profiles and the mass flux in the wind. If the flow time is much greater than the heating time, a narrow transition between the photosphere and the corona occurs. Otherwise the transition is gradual. If the escape temperature is small compared to the X-ray temperature, the sonic point occurs at a height small compared to the coronal pressure scale height. The density is relatively high, and the mass flux is large. If the escape temperature is high, the corona is nearly static and isothermal with an exponential decay of density prior to the sonic point; in this case, the mass flux is small. We locate the known X-ray binary systems in the parameter space of our model and estimate the mass-loss rates from them.

Subject headings: hydrodynamics — stars: binaries — stars: winds — X-rays: binaries

I. INTRODUCTION

Winds from the normal stars in X-ray binary systems are a source of matter to power the X-ray emission. They may also play a role in the evolution of the systems by carrying away mass and angular momentum. The X-ray illumination of the stellar atmosphere can greatly influence the wind. The effect is of interest mainly in late-type stars in which the intrinsic mass loss may be small and in which the X-rays have a large effect on the normal star's atmosphere. There are five such systems known, and approximately 20 of the 100 known optical counterparts of X-ray sources have X-ray luminosity greater than optical and are candidates for such processes (Bradt, Doxsey, and Jernigan 1979).

In this paper we deal with the calculation of the structure and mass loss of a stellar wind, given the binary separation, and the stellar sizes, masses, and luminosities. In a previous paper, London, McCray, and Auer (1981, hereafter LMA) point out that the general problem of X-ray illuminated stellar atmospheres can be divided into two parts (see also Anderson 1981). This is possible because a narrow transition zone divides the atmosphere into a photosphere-chromosphere region and a corona, much like the solar atmosphere. The lower region is nearly static, and its structure is not affected by the optically thin corona. They determined the structure of the lower atmosphere and the location of the transition region with a hydrostatic, thermal equilibrium radiative transfer model. In this paper we address the second part of the problem: the structure of the outflowing corona. This requires solving hydrodynamic equations, since the flow velocity becomes supersonic, and dynamic terms in the momentum and energy balance are important. The radiation field in the corona can be specified from the results of the lower atmosphere models. The approximation of an optically thin corona is checked for consistency after the calculations.

Although models for X-ray induced stellar winds have been presented previously, we feel that no model has yet incorporated an accurate treatment of the hydrodynamics, the essential physical processes, and a clear discussion of the relationship of the input physics to the solutions. Our goal in this paper is twofold: we present a new technique for solving steady state flow problems with sonic transitions, and we present accurate solutions of the hydrodynamic equations for this problem from which the relationship of input parameters to the results is easily shown. Although we shall estimate mass-loss rates, we do not claim them to be extremely accurate because we make simplifications in the atomic physics and geometry to render this problem tractable.

With this goal in mind, we shall ultilize an idealized model for the atomic processes involved in heating and cooling the gas. This model, described in § II, has a few parameters whose values we choose to account for the important atomic contributors to the energy exchange in a radiation field as calculated by LMA. The advantage of using the simplified model is that the physical behavior of the flowing gas can be clearly understood. We find that the results depend on only three dimensionless parameters, which are ratios of characteristic temperatures and time scales. By estimating these temperatures and time scales for more realistic physics, we can apply our findings to a more realistic model.

Before we describe our model in detail, let us discuss some of the past work in order to explain why we take another look at this problem.

Early work by Arons (1973), Basko and Sunyaev (1973), and McCray and Hatchett (1975) first suggested the importance of the X-ray induced wind. Two more recent papers deal with the problem in somewhat more detail.

Alme and Wilson (1974) present a very detailed gas dynamic model for X-ray induced winds. They solve one-dimensional, time dependent, coupled, radiative transfer, and hydrodynamic equations using a sophisticated numerical code. Using physical parameters appropriate to the HZ Her system, they examine how the mass flux in steady state, relaxed solutions varies with the incident X-rays, the abundance of the heavier elements, and the distance from the photosphere to the gravitational saddle (L_1) point in a Roche potential. Although they describe the general trends of the calculations, they do not provide a clear description of the connection between the results and the input physics. An additional problem with their calculations is that in certain cases they find persistent oscillations in the solutions which they cannot explain in physical terms.

Basko *et al.* (1977) give a clear picture of some of the underlying physics of the wind. They point out the two distinct zones in the atmosphere: the photosphere and corona. By assuming that the flow in the corona is isothermal, they estimate the mass loss. Their argument is based on guesses of heating and flow time scales, and they claim their results are uncertain to a factor of 3. They do not solve the flow equations but only suggest how their approximation could be improved by knowing the correct time scales.

We proceed in this paper to present the details of our model and the method of solution in § II, the solutions and discussion in § III, and a discussion of the application of our model to the X-ray binaries in § IV.

II. THE WIND MODEL

a) *Description and Equations*

We consider one-dimensional, plane-parallel flow in a gravitational field appropriate to the region near the L_1 point in a Roche potential. We assume that the stellar surface, defined by the location of the transition region, is at a significant distance from the L_1 point so that there is no Roche lobe overflow at the photospheric temperature. We solve the steady flow equations describing the gas structure as a function of distance from the star, looking for wind solutions which have free streaming far from the surface. In effect, the possibility of a subsonic settling solution on the compact star is ignored. We consider heating by X-ray and ultraviolet radiation but ignore radiation pressure. Thermal conduction is not important as it is in the solar corona, since the X-ray heating dominates the energy balance. We ignore Coriolis forces. The appropriate equations for conservation of mass, momentum, and energy are:

$$\frac{d}{dz}\rho v = 0\,, \tag{1}$$

$$\frac{d}{dz}(P + \rho v^2) = -\rho g\,, \tag{2}$$

$$\frac{d}{dz}\left[\rho v\left(\frac{5}{2}\frac{P}{\rho} + \frac{1}{2}v^2 + \phi\right)\right] = \rho\mathscr{L}\,. \tag{3}$$

Here the independent variable z measures height above the stellar surface; ρ, v, and P are the density, velocity, and pressure of the gas; g and ϕ are the gravity and gravitational potential; and $\mathscr{L}$ is the net radiative heating per unit mass. The gas temperature, T, is found from the equation of state:

$$T = \frac{m_p P}{2\rho k}\,, \tag{4}$$

where m_p is the proton mass. We have assumed an ionized hydrogen plasma. With a suitable definition of mean atomic weight, this could be generalized to include the contribution of helium.

For the gravity, we use a first-order expansion of the effective gravity along the line of centers in the Roche potential:

$$g = g_0\left(1 - \frac{z}{z_0}\right). \tag{5}$$

This is accurate as long as $z_0 < 0.2$ A, the binary separation. The potential is quadratic in z with a maximum at $z = z_0$.

We model the heating by a simple analytic formula including X-ray heating by either photoionization of the heavy elements (C, N, O, Fe, etc.) or Compton scattering (cf. London 1979) and continuum radiative processes of hydrogen. The X-ray heating is given by:

$$\mathscr{L}_x = \mathscr{L}_{x_0}\left(1 - \frac{T}{T_x}\right). \tag{6}$$

The value at low temperature, $\mathscr{L}_{x_0}$, is calculated from the X-ray flux and spectrum. The heating cuts off at high temperature, as $T \to T_x$. The value of T_x depends on the X-ray spectral temperature when modeling Compton heating, or the low-energy X-ray spectrum and the atomic cross sections and abundances when modeling photoionization. The second part of the net heating is

due to photoionization and recombination of hydrogen:

$$\mathscr{L}_{\rm H} = \frac{1}{m_p}\left[\tfrac{1}{2}\alpha_0 P T^{-3/2}(T_R - T)\right] . \quad (7)$$

Here α_0 is the recombination constant (recombination rate coefficient is $\alpha_0 T^{-1/2}$), and T_R is the radiation temperature of the photosphere ($T_R \approx 10^4$ K). We have assumed, in writing equation (7), that the ionized fraction of hydrogen is determined by a balance of photoionization and radiative recombination. The photoionization is dominated by the photospheric (mostly reprocessed X-rays) radiation, rather than the incident X-rays. At high temperature $\mathscr{L}_{\rm H} =$ constant $\times\ T^{-1/2}$, approximating bremsstrahlung cooling.

The important feature of the heating function is the shape of the thermal equilibrium curve. In Figure 1 we show the equilibrium temperature at which $\mathscr{L} = 0$, as a function of pressure. At high pressure (deep in the atmosphere) $T \to T_R$. At low pressure (high in the atmosphere) $T \to T_X$. In between there is a region where the temperature has three equilibrium values at a given pressure. The middle solution is unstable. The correct choice between the other two depends on the thermal history of the gas. In the case of outflow from high to low pressure, a transition from T_R to T_X takes place in a thin zone near the pressure $P_{\rm min} = 3^{3/2}P_0$, where P_0 is the pressure scale defined below.

A more realistic treatment of the heating and cooling gives the same qualitative behavior, with perhaps several twists in the equilibrium curve (cf. McCray and Hatchett 1975; Kallman 1980).

To facilitate finding and understanding solutions of the flow equations, we reduce them to nondimensional form.

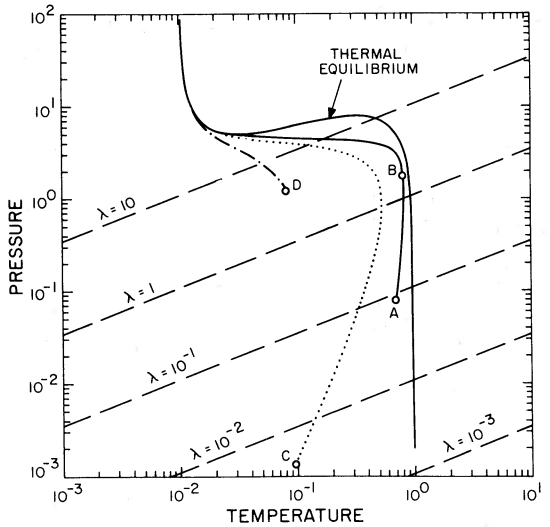

FIG. 1.—Pressure-temperature curves. We show the dimensionless pressure and temperature defined in § IIa. The solid curve labeled "thermal equilibrium" is derived by setting the net heating equal to zero. The other curves are the results of the model calculations. The sonic point of each model is labeled by the letter used in Table 1. The diagonal-dashed lines are mass flux contours specifying the pressure and temperature at the sonic point for given values of λ.

We scale the distance to z_0, temperature to T_X, velocity to $v_0 \equiv (kT_X/m_p)^{1/2}$, and pressure to

$$P_0 = \frac{m_p \mathscr{L}_{x_0} T_R^{1/2}}{\alpha_0} . \quad (8)$$

The natural density scale is then $\rho = m_p P_0/kT_x$. The mass flux scale is

$$\lambda_0 \equiv \rho_0 v_0 \equiv P_0\left[\frac{kT_X}{m_p}\right]^{-1/2} . \quad (9)$$

The scale for the gravity is the surface value g_0, and for the potential it is $\phi_0 \equiv g_0 z_0$ (twice the potential from the surface to the L_1 point). After dividing out the scale factors we are left with three nondimensional parameters in the equations. These are chosen to be:

$$R_1 = T_x/T_R, \quad R_2 = T_x/T_\phi, \quad \text{and} \quad R_3 = \tau_F/\tau_H . \quad (10)$$

Here $\tau_F = z_0/v_0$ is a time characteristic of the flow, τ_H is a time characteristic of heating, and T_ϕ is a temperature characteristic of the potential drop from L_1 to the stellar surface. Note that at T_ϕ the thermal energy of the gas per unit mass ($3kT/m_p$) exceeds the energy required to escape from the gravitational potential ($\phi/2$) by a factor of 6. Thus, when R_2 is small the potential barrier is high, and when R_2 approaches unity the potential barrier is shallow (for gas at $T = T_x$). The actual temperature at which gas reaches the sonic point depends on additional interactions, especially on R_3 which determines whether or not heating, or adiabatic cooling, can occur.

Using the same symbols for the physical variables as in equations (1–3) and the scaling described in the previous paragraph, and introducing the dimensionless mass flux λ, we write the nondimensional wind equations as follows:

$$\frac{d}{dz}\lambda = 0 , \quad (11)$$

$$\frac{d}{dz}\left(P + \frac{\lambda^2}{\rho}\right) = -\frac{\rho g}{R_2} , \quad (12)$$

$$\frac{d}{dz}\left[\lambda\left(\frac{5}{2}\frac{P}{\rho} + \frac{1}{2}\rho^{-2} + \frac{\phi}{R_2}\right)\right] = R_3 \rho \mathscr{L} . \quad (13)$$

The dimensionless heating function is

$$\mathscr{L} = \left(1 - T\right) + \frac{1}{2}P(TR_1)^{-1/2}\left(\frac{1}{TR_1} - 1\right) . \quad (14)$$

The equation of state is

$$T = \frac{1}{2}\frac{P}{\rho} . \quad (15)$$

Equations (11), (12), and (13) are three coupled first-order equations with dependent variables P, ρ, and λ. We seek solutions which match the hydrostatic stellar atmosphere at the surface and are supersonic at large distance from the star. We must specify three boundary conditions to find a unique solution. Two boundary conditions are

applied at the surface. We choose the pressure there and also require thermal equilibrium ($\mathscr{L} = 0$). The exact choice of pressure is unimportant as long as the flow speed is small compared to the sound speed and the local thermal time scale is short compared to the flow time scale. This requires choosing the pressure about a factor of 2 larger than $P_{\min}$. In fact, with such a choice of pressure, the requirement of thermal equilibrium is not important since the gas would reach equilibrium quickly in any case. The third boundary condition is applied at the sonic point. By combining equations (11–13) we find that the following condition is necessary to ensure a regular solution when the adiabatic Mach number is unity:

$$R_2 R_3 \rho \mathscr{L} = -\tfrac{3}{2}\lambda g \,. \tag{16}$$

b) Numerical Techniques

Because a singularity occurs in the differential equations at the sonic point, standard methods often fail to provide accurate solutions for the transonic wind. The correct solution is characterized by a transition to supersonic flow at the sonic point z_s, and a unique mass flux λ_s, but *a priori* neither z_s nor λ_s are known.

However, given a set of surface boundary conditions, e.g., $P(0)$, $\rho(0)$, and λ, the coupled, ordinary, differential equations can be solved as an initial value problem. As the integration proceeds outward and the Mach number approaches unity, the influence of the singularity forces the solution into an unphysical regime, unless the sonic condition (eq. [16]) is precisely satisfied. One standard technique for these problems, the "shooting method," uses this approach; one seeks to satisfy the sonic condition by iteratively correcting the trial surface boundary conditions. This method readily determines the mass flux with high accuracy, but often fails to determine the location of the sonic point to even a few percent: that is the case here.

Rather than approaching the equations as an initial value problem with an adjustable parameter, we have developed a method which treats the equations as a two-point boundary value problem. We use a relaxation technique, as described in Kippenhahn, Weigert, and Hofmeister (1968), which replaces the differential equations with algebraic difference equations on a finite mesh. The solution consists of a set of variables, defined at each point in the mesh, from which we can calculate terms in the difference equations. Given an initial trial solution, we iteratively improve the solution using a Newton-Raphson procedure until the equations are satisfied to some tolerance. The difficulty with applying relaxation here is that the location of the sonic point is not known, so the spatial range of the mesh cannot be preset. We use an approach similar in spirit to Eggleton's (1971) formulation of the stellar structure relaxation problem on a non-Lagrangian grid. At the expense of introducing two additional differential equations, we transform to a new independent variable, $q(z)$, which gives us the freedom to adjust the mesh and to impose the sonic boundary condition directly.

We define a transformation which allows us to express a differential equation with respect to z in terms of a new independent variable q. For example the equation

$$\frac{dF}{dz} = G \tag{17}$$

is transformed to

$$\frac{dF}{dq} = G\frac{dz}{dq} \,. \tag{18}$$

We construct the transformation by first specifying a "mesh spacing function," $Q(z)$, which is monotonic, has a known derivative with respect to z, and increases by a constant amount, ψ, between mesh points. The following equations describe this function:

$$\frac{dQ}{dq} = \psi \tag{19}$$

and

$$\frac{d\psi}{dq} = 0 \,. \tag{20}$$

Since we require that $Q(z)$ have a known derivative

$$\frac{dQ}{dz} = \theta(z) \,, \tag{21}$$

the transformation from z to q can be written as

$$\frac{dz}{dq} = \frac{dQ}{dq}\frac{dz}{dQ} = \frac{\psi}{\theta} \,. \tag{22}$$

It is convenient to scale the continuous variable q as an index which labels the mesh points, i.e., for an N-point grid, $q = 1, 2, 3, \ldots N$ at the mesh points. This can be done by appropriately scaling ψ.

As an example, first consider the case of the wind equations as an initial value problem, without a sonic point, on the interval $z_1 < z < z_2$, with, for instance, $Q(z) = \log z$. The overall problem consists of the two mesh spacing equations (eqs. [19] and [20]) plus the three wind equations (eqs. [11–13]) transformed from z to q as independent variable. In this case the five boundary conditions on the N-point mesh are at $q = 1$:

$$z = z_1 \,, \quad P = P_1 \,, \quad \mathscr{L} = 0 \,, \quad \text{and} \quad \lambda = \lambda_0 \,, \tag{23}$$

and at $q = N$:

$$z = z_2 \,. \tag{24}$$

An appropriate choice of variables to define the solution at each point in the grid might be: λ, P, ρ, z, and ψ. Little has been gained here except for logarithmic mesh spacing in z, which might be of some advantage.

The utility of the method becomes apparent when one considers the transonic wind problem. Here we replace two of the previous boundary conditions, on mass flux (eq. [23]), and on the physical location of the outer edge of the grid (eq. [24]), by the two sonic conditions at $q = N$:

$$\mathscr{M} = 1, \quad \text{and} \quad R_2 R_3 \mathscr{L} = -\tfrac{3}{2}\lambda g \,, \tag{25}$$

where $\mathcal{M}$ is the adiabatic Mach number [$\mathcal{M} \equiv V/(5/3P/\rho)]^{1/2}$. Note that neither the location of the sonic point $z(N)$ nor the mass flux λ needs to be specified. Nonetheless, the algebraic relations given by the finite difference representation of the equations and boundary conditions lead to a unique solution. As the iterations proceed, both λ and the spacing of the mesh are simultaneously adjusted to satisfy the constraints at the surface and the sonic point.

In practice, we use logarithmic variables and a more complicated formula for the mesh spacing which allows us to resolve the narrow transition region. We start the relaxation scheme with an initial trial solution, obtained from a Runge-Kutta integration, in which the Mach number at the outer edge of the grid is ~ 0.8. Typically, during iterations the edge of the grid, z_s, will adjust by as much as 50%, and the model will converge to the true solution in only three or four iterations. The solution valid for one set of parameters (R_1, R_2, and R_3) can serve as an initial guess for a moderately perturbed ($\Delta R_i < 30\%$) new set of parameters.

III. RESULTS OF MODEL CALCULATIONS

a) Solution Space

Using the numerical techniques described above, we have explored the two-dimensional solution space of the wind equations generated by varying $R_2 = T_x/T_\phi$ and $R_3 = \tau_F/\tau_H$, as shown in Figure 2. We have examined the effects of varying $R_1 = T_x/T_R$ by computing several models with $10^2 \leq R_1 \leq 10^3$. We find that the exact value does not qualitatively change the solution, nor does it change the mass flux by more than 25%. We therefore keep R_1 fixed at a value of 100 since we expect it to be of this order or larger in all cases of interest.

In Table 1 we show the parameters and important results for four models with R_2 and R_3 taking on values of 0.1 and 10. These models demonstrate the typical range of behavior of solutions. The solutions take on asymptotic behavior which we can describe analytically for values outside this range. In Figure 3 we show the temperature and pressure profiles of these models. The pressure at the surface was fixed at the same value for all models. It decreases outward in all cases. Larger decreases in pressure result in lower mass flux. The temperature profiles in models A, B, and C are similar in that they have a sharp rise from $T \approx T_R$ to $T \approx T_X$ at a pressure approximately equal to $P_{\min}$. This can be understood by looking at Figure 1, where we show curves of pressure versus temperature for the models as well as for thermal equilibrium. The transition region is not at the same position for all models in Figure 3 (it depends on $R_2 = T_x/T_\phi$) because of the choice of the distance scaling factor. The temperature drop in Model C near $z = 1$ is due to expansion cooling. In Model D the temperature never approaches T_X because the flow goes supersonic at $T \approx T_\phi$ which is $0.1T_X$. Figure 4 shows the Mach number profiles. We note that the curves all end at $\mathcal{M} = 1$, as specified by our boundary conditions. Figure 5 shows λ, the dimensionless mass loss, as a

TABLE 1

FOUR LIMITING MODELS

Model	$R_2(T_x/T_\phi)$	$R_3(\tau_F/\tau_H)$	λ	T_s[a]	Z_s
A	0.1	10	0.092	0.71	1.26
B	10	10	1.910	0.84	3.31
C	0.1	0.1	0.0039	0.094	1.01
D	10	0.1	4.090	0.083	1.92

[a] Temperature at the sonic point.

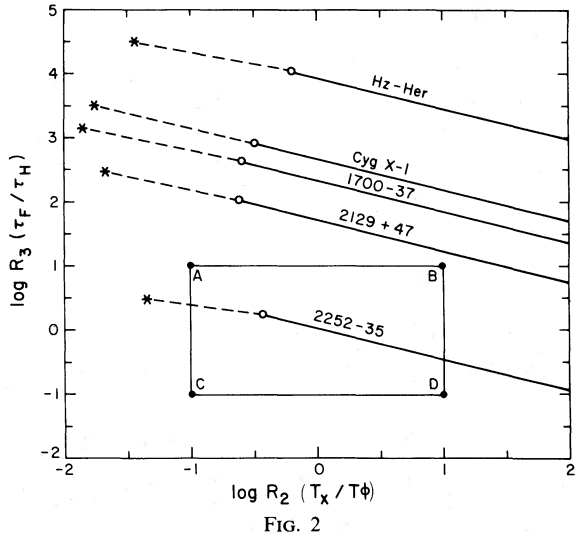

FIG. 2

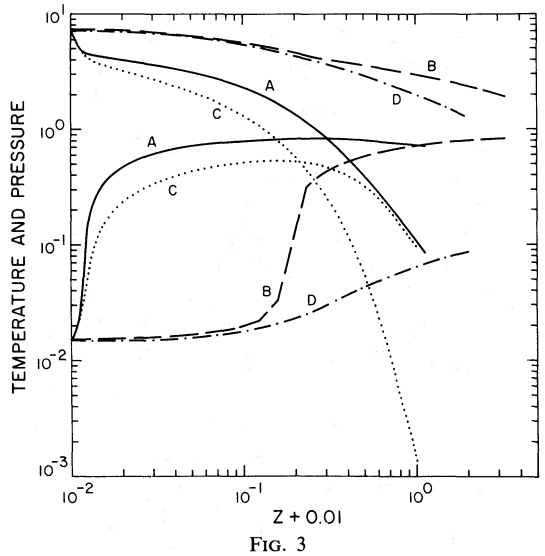

FIG. 3

FIG. 2.—Solution parameter space. The filled circles are the models in Table 1, the stars are the positions of the binary systems in Table 2 using the unperturbed gravity. The open circles are for the binary systems with the flow assumed to be along the line of centers and the parameter $\Delta = 0.1$. The lines adjoining the circles indicate the values of the parameters as Δ is lowered from 0.1. T_X is taken to be 10^6 K.

FIG. 3.—Pressure and temperature profiles for four wind models lettered according to Table 1

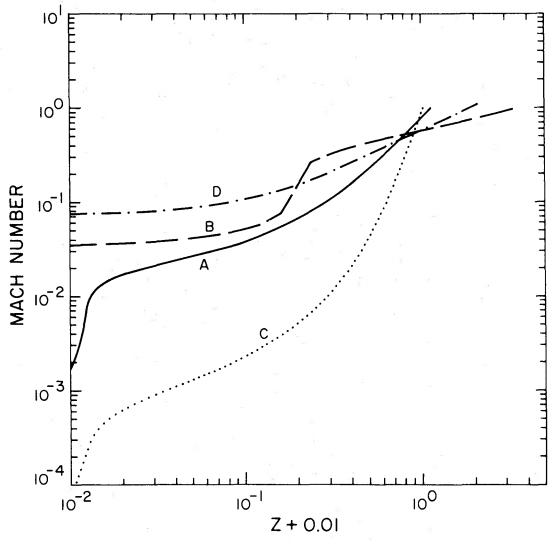

FIG. 4.—We show the adiabatic Mach number profiles of the four models labeled according to Table 1

function of R_2 for three values of R_3. We now proceed to discuss the four limiting solutions in slightly greater detail.

b) $\tau_F \gg \tau_H$: Models A and B

In models A and B, $\tau_F = 10\tau_H$, and the heating is so fast that the temperature jumps to a value near T_X in the transition region and remains there throughout the corona. The mass flux can be estimated with an isothermal wind model. Following Basko *et al.* (1977), we find the transonic solution of the continuity and momentum equations (eqs. [11] and [12]) with constant temperature T_X. By applying jump conditions across the transition region, the mass flux can be expressed as:

$$\lambda = 3(\tfrac{3}{2})^{1/2} \frac{\mathcal{M}_0}{1 + \mathcal{M}_0^2} . \quad (26)$$

Here $\mathcal{M}_0$ is the *isothermal* Mach number at the base of the corona. It is found from the following algebraic relation, derived from the flow equations:

$$\mathcal{M}_0^2 - \ln \mathcal{M}_0^2 = 1 + (z^2 - z + 1)/2R_2 . \quad (27)$$

For $T_X \ll T_\phi$, we find:

$$\lambda \approx 3(\tfrac{3}{2})^{1/2} \exp(-1/4R_2) . \quad (28)$$

In this case, which corresponds to model A, the thermal energy of the gas in the lower corona is less than that needed to escape; we therefore have a hydrostatic region in which the pressure drops exponentially. Only when the gas gets close enough to the L_1 point to escape at T_X does the Mach number approach unity. The mass flux is small in this limit and drops exponentially as T_x/T_ϕ gets larger.

For $T_X \gg T_\phi$, equation (26) gives $\lambda \approx 1.84$. This corresponds to Model B. Note that our model breaks down as T_ϕ is lowered beyond $0.1T_X$ and, therefore, approaches T_R. In that case, the star would fill its Roche lobe and spill over the saddle with very little heating. There is good agreement between the analytic results and the numerical results for models A and B.

c) $\tau_F \ll \tau_H$: Models C and D

In Model C with $\tau_F = 0.1\tau_H$, adiabatic cooling is important in the corona. Even though the flow time is "short," the gas heats to T_x in the lower corona. This occurs because, when $T_x \ll T_\phi$, the Mach number remains small in the transition region, thus prolonging the residence time long enough for heating to occur. Higher up in the corona, where the local escape temperature drops to T_X, the gas picks up speed and flows out. Then the gas cools adiabatically because the flow time becomes shorter than the heating time. In the adiabatic region, the pressure drops faster; the mass flux in this limit is very small.

The final case is Model D with $T_X \gg T_\phi$. At pressures lower than $P_{\min}$, the gas heats toward T_X. Since the flow time is short compared to the heating time, Tapproaches T_ϕ and the gas flows over the saddle point. Here the mass loss is large, $\lambda = 4.09$. In fact, this case is close to Roche lobe overflow, since the thermal energy of gas at the stellar surface nearly equals the gravitational binding energy. Nonetheless, the calculation remains consistent, since the Mach number is small at the surface. To test whether or not X-ray heating was essential to outflow in case D, we examined another model with the same value for T_X/T_ϕ, but with T_X/T_R increased to 1000, so that the gravitational barrier would be greater with respect to the surface temperature. This reduced the rate of mass loss by only 25%, which indicates that X-ray heating was significant in case D. As T_X/T_ϕ gets even larger, so

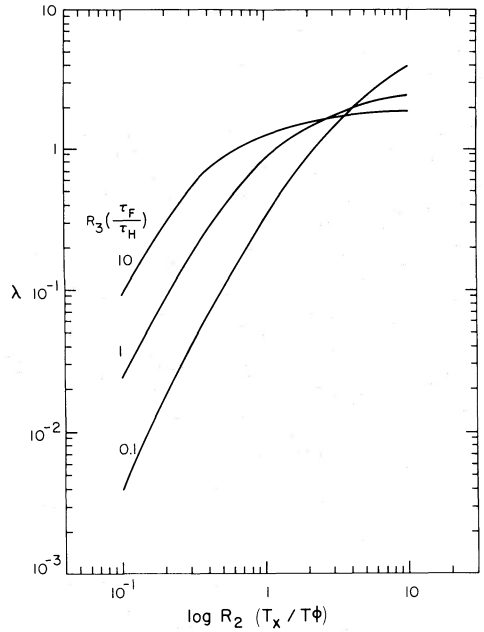

FIG. 5.—The dimensionless mass flux for several values of R_3 is plotted as a function of R_2

that $T_\phi \approx T_R$, the mass flux approaches the limiting value of 10. This is because the scale for the mass flux becomes dependent on the sound speed at T_R rather than at T_X (see eq. [9] for the mass flux scale). At this point our assumptions break down, since we have bona fide Roche lobe overflow with significant flow velocity at the surface.

d) *Relationship to Spherical Winds*

Basko *et al.* (1977) discuss isothermal winds similar to our models A and B in plane-parallel and spherical geometry. As they show, the isothermal solutions are similar in the different geometries if one uses the appropriate dimensionless parameters. There is, however, a misunderstanding in the paper by Basko *et al.* in locating the sonic point for a spherical wind corresponding to our model B, which we wish to clarify. In plane-parallel winds, the sonic point occurs at or beyond the saddle point at $Z = 1$. This can be deduced from equation (16), knowing that the net heating is always positive. However, in spherical isothermal winds, the sonic radius is $R_S = GMm_p/4kT$. For $T > T_\Phi$, this condition gives a sonic point inside the star, which is incompatible with the actual temperature below the transition region, of order T_R. At T_R the isothermal sonic point is far outside the surface. Basko *et al.* claim that the temperature will jump in the transition to T_Φ and then slowly increase to T_X, with the sonic point occurring at some distance above the surface. This is incorrect. The condition $\tau_F \gg \tau_H$ ensures that the temperature rises to T_X in a distance much smaller than the stellar radius.

The situation is shown in Figure 6, where we plot the velocity squared versus the radius for spherical isothermal flows at temperatures T_R and T_X. The usual critical point solution topology (cf. Parker 1963) is evident. For $T = T_X = 10T_\phi$, the sonic point would be inside the star, while for $T = T_R = 1/10T_\phi$, it would be outside. The transition from T_R to T_X is fixed by the local pressure and occurs slightly above the stellar surface.

The correct solution follows a subsonic branch at T_R and then jumps to a barely supersonic branch at T_X. This supersonic branch is one which does not represent a valid solution in a strictly isothermal wind since it does not reach the stellar surface. Only with a temperature jump can the gas get to this branch.

We may find the location of the sonic point analytically by considering the continuity and momentum equations in a similar manner to the isothermal wind, but with an appropriate *nonconstant* temperature profile (Holzer 1980). In this case, the sonic condition is found to be:

$$R_s = \frac{GMm_p}{2kT} + \frac{R_s}{2}\frac{d \ln T}{d \ln R} . \quad (29)$$

Using a temperature profile that has a steep, but smooth, transition from T_R to T_X, and with $T_X \gg T_\phi \gg T_R$, we find that the sonic point occurs near the top of the transition zone where $T \approx T_X$ and $d \ln T/d \ln R = 2$. In this case the mass flux is

$$\lambda = (\tfrac{3}{2})^{3/2} = 1.8 . \quad (30)$$

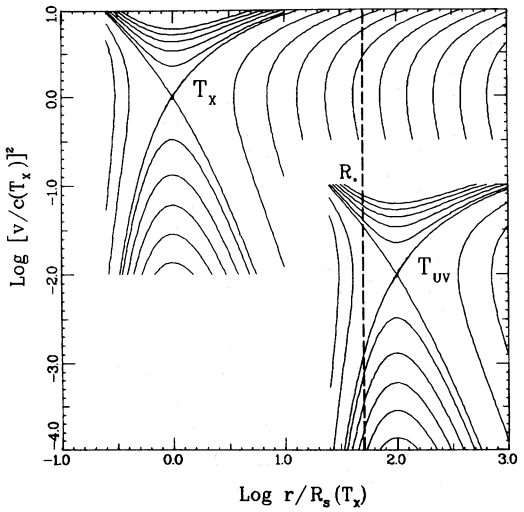

FIG. 6.—Critical point topology for isothermal transonic winds in spherical geometry with units scaled relative to the sound speed and sonic radius at the X-ray temperature. Using the approximations in eq. (31) to extend our definitions of parameters to spherical geometry, we locate the stellar radius at $R_* = 8T/T_\phi$. (The heavy, dashed line indicates R_* when $T/T_\phi = 6.3$.) Schematically, in our case B ($T_x = 10T_\phi$, $\tau_F = 10\tau_H$) a nonadiabatic solution could be approximated by two isothermal segments. Flow leaves the star along a subsonic branch appropriate to T_R and encounters the chromospheric transition once the pressure drops below P_{min}. The gas then heats to T_X in a short distance, passing through the sonic point during the thermal transition. The flow matches onto the outflowing section of the appropriate double-valued, high-temperature solution. That section does not join with the origin and would be inaccessible without heating.

e) *Comparison to Previous Work*

We wish briefly to compare our one-dimensional hydrodynamic models with previous results. Basko *et al.* (1977) derive a formula for mass flux from an isothermal corona, which they apply to the case of HZ Her. However, in their discussion they seem to claim that the approximation of isothermal spherical winds is valid in the limit $\tau_F \ll \tau_H$ and can be applied to HZ Her. Thus, we agree with their formula and its application, but find that their range of validity was incorrectly stated and, for them, incorrectly applied. The results of Alme and Wilson (1974) are similar to ours, but they only consider cases with $T_x \gg T_\phi$.

IV. MASS LOSS IN BINARY SYSTEMS

To estimate the mass loss for real systems, we first estimate the parameters R_1, R_2, and R_3. From these and the results of § III (i.e., Fig. 5), we estimate the mass flux in the wind. Then, using the geometrical parameters of the binary systems, we estimate the area over which this mass loss takes place and, thereby, a mass-loss rate.

a) *Model Parameters*

As we discussed in § II, T_R is typically 10^4 K, while T_X is 10^6 K or 10^7 K. Therefore, R_1 is always large and its precise value is not important. We can estimate R_2 and R_3 in two ways.

The first method, which we call case I, assumes that the normal star is unperturbed by its companion and the gravity has the usual inverse square dependence. In this case,

$$T_\phi = 2\frac{GMm_p}{kR}, \quad \text{and} \quad \tau_F = \frac{R}{v_0}, \tag{31}$$

where M is the stellar mass and R its radius. We then use equations (10) to find:

$$R_2 \equiv \frac{T_X}{T_\phi} = 2.1 \times 10^{-2}\left(\frac{T_X}{10^6}\right)\left(\frac{R}{R_\odot}\right)\left(\frac{M}{M_\odot}\right)^{-1}, \tag{32}$$

$$R_3 \equiv \frac{\tau_F}{\tau_H} = 9.3 \times 10^3\left(\frac{T_X}{10^6}\right)^{-3/2}\left(\frac{R}{R_\odot}\right)\left(\frac{\mathscr{L}_{x_0}}{10^{14}}\right). \tag{33}$$

These estimates apply when the star is well inside its critical Roche lobe. Here the wind will blow from the illuminated surface in an almost uniform manner. This also may be used for a crude estimate of the mass flux in the wind from surface points away from L_1, even when the star nearly fills its critical lobe.

In case II, we consider the flow along the line of centers for a star close to filling its critical Roche lobe. We measure the escape potential from the surface to the L_1 point as in the original definition of T_ϕ in § II. The first-order expansion of the gravity near L_1 is:

$$g = \alpha(f)\Delta\frac{GM}{A^2}, \tag{34}$$

where $f = M/(M + M_X)$ is the mass fraction in the normal star, M_X being the mass of the compact component. Here, α is an expansion coefficient shown in Figure 7, A is the binary separation, and Δ is the distance from the L_1 point divided by A. To ensure the validity of equation (34), we limit ourselves to $\Delta < 0.2$.

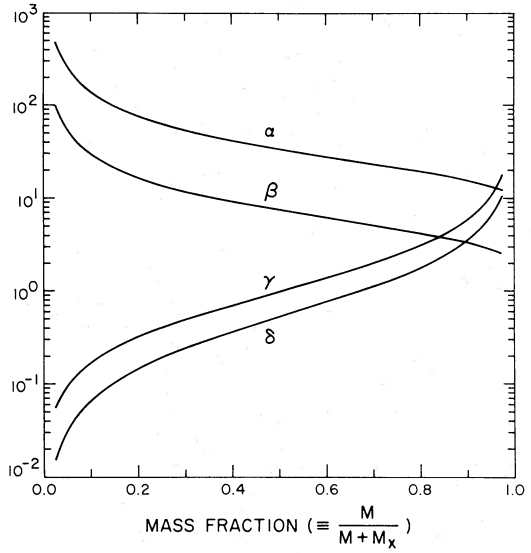

FIG. 7.—Dimensionless geometrical functions for the Roche potential used for estimating R_2, R_3, and mass-loss rates plotted vs. binary mass fraction

Using the original definitions of T_ϕ and τ_F in § II, we find parameters:

$$R_2 \equiv \frac{T_X}{T_\phi} = 4.3 \times 10^{-2}\left(\frac{T_X}{10^6}\right)\left(\frac{A}{R_\odot}\right)\left(\frac{M}{M_\odot}\right)^{-1}\alpha^{-1}\Delta^{-2}, \tag{35}$$

and

$$R_3 = \frac{\tau_F}{\tau_H} = 9.3 \times 10^3\left(\frac{T_X}{10^6}\right)^{-3/2}\left(\frac{A}{R_\odot}\right)\left(\frac{\mathscr{L}_{x_0}}{10^{14}}\right)\Delta. \tag{36}$$

A given binary system traces out a curve with $R_3 \propto {R_2}^{-2}$, as we vary Δ as shown in Figure 2 for several binary systems.

In Table 2 we list physical parameters for several systems. The first three systems are low-mass binaries in which the X-ray induced wind may be important, while the last two entries are higher mass systems in which the intrinsic stellar wind is probably larger. We have calculated the X-ray heating constant using the X-ray luminosity (L_X) and the distance from the X-ray source to the surface (D) with the following formula:

$$\mathscr{L}_{X_0} = 6.0\frac{L_X}{4\pi D^2}y, \tag{37}$$

where y is a dimensionless factor which depends on the X-ray spectrum. The details of the calculation of the heating rate are discussed by LMA. We have designed this formula so that y is 1 for a 20 keV exponential spectrum. The value is mainly sensitive to the soft X-ray flux of the source.

In Figure 2 we show the values of R_2 and R_3 for the systems listed in Table 2. The stars indicate the values using the unperturbed gravitational potential (eqs. [32] and [33]), while the circles indicate the positions using equations (35) and (36) with $\Delta = 0.1$. The lines show the values as Δ is lowered, representing the stars getting closer to their critical lobes.

b) *Integral over the Surface*

The final step in calculating the mass loss is to integrate the mass flux over the stellar surface:

$$\dot{M} = \int \rho v dS. \tag{38}$$

The mass-loss problem is really a three-dimensional one. There is no plane-parallel symmetry, and radiation and Coriolis forces may be important in a binary star. Also, nonsynchronous rotation would alter the boundary conditions used here. We make a very rough estimate of the mass loss and the fraction transferred to the compact star by considering the two limiting cases described above in the calculation of the dimensionless parameters. We approximate equation (38) by

$$\dot{M} = (\rho v)_{\text{ave}}\Delta S. \tag{39}$$

In the first case, we consider the "hemispherical" mass loss from a detached star. The appropriate area here is that illuminated by X-rays: about $\frac{1}{4}$ of the stellar surface

TABLE 2

ADOPTED PARAMETERS AND ESTIMATED MASS-LOSS RATES FOR X-RAY BINARIES

Source	$M/M_\odot$	$M_x/M_\odot$	L_x (ergs s^{-1})	A (cm)	L_{x_0} (ergs g^{-1} s^{-1})	$\dot{M}_{\rm I}$ (g s^{-1})	$\dot{M}_{\rm II}$ (g s^{-1})	$\dot{M}_x$ (g s^{-1})
HZ Her-Her X-1[a]	2.2	1.3	2×10^{37}	6.3×10^{11}	1.2×10^{14}	3.9×10^{16}	7.7×10^{17}	2.2×10^{17}
2129+47[b]	0.65	1.3	6×10^{34}	1.3×10^{11}	4.8×10^{12}	8.7×10^{10}	2.1×10^{14}	6.7×10^{14}
2252−35[c]	0.1	1.0	1×10^{33}	8.3×10^{10}	1.4×10^{11}	1.4×10^{12}	2.2×10^{12}	1.1×10^{13} 1.1×10^{15}[d]
1700−37[e]	27	1.3	6×10^{35}	2.0×10^{12}	1.3×10^{12}	1.6×10^{11}	2.5×10^{16}	6.7×10^{15}
Cyg X-1[e]	21	13.0	7×10^{36}	3.0×10^{12}	1.8×10^{12}	2.7×10^{13}	7.8×10^{16}	7.5×10^{16}

[a] Cf. LMA.
[b] Thorstensen *et al.* 1979, McClintock, Remillard, and Margon 1981.
[c] Patterson and Price 1981; Patterson and Jablonski 1981.
[d] Assuming the compact star is a white dwarf.
[e] Conti 1978.

area. Most of this mass loss will escape the system. The calculation of the fate of this matter is complicated. We estimate the fraction captured by the compact star by applying a theory for accretion by a star from a uniform, plane-parallel flow (cf. McCray and Hatchett 1975):

$$\left(\frac{\dot{M}_{\rm cep}}{\dot{M}}\right) = 5 \times 10^{-2}\left(\frac{M_X}{M_\odot}\right)^2\left(\frac{T_f}{10^7}\right)^{-2}\left(\frac{D+R}{10R_\odot}\right)^{-2}, \quad (40)$$

where T_f is the final temperature of the wind, of the order of the X-ray spectral temperature (generally $>10^7$ K).

In case II, the appropriate area may be estimated by assuming that near L_1 the wind extends perpendicular to the line of centers to a distance at which the gravitational potential relative to that at L_1 is equal to thermal energy (cf. Lubow and Shu 1975). We then find an area:

$$\Delta S_{\rm II} = \pi A^2\left(\frac{kT_X}{GMm_p/A}\right)\beta(f), \quad (41)$$

where $\beta(f)$, shown in Figure 7, is derived from a second-order expansion of the Roche potential near L_1.

By combining equation (9) for the mass flux scale with equation (37) for the X-ray heating rate and the area factors, we now estimate the mass loss for cases I and II. We define dimensionless mass-loss rates, $\dot{\mu}$, by dividing $\dot{M}$ by $\dot{M}_X \equiv L_X/ec$, the accreted mass needed to power the X-ray emission. We find for the two cases of mass loss:

$$\dot{\mu}_{\rm I} = 24\lambda y\gamma\left(\frac{T_X}{10^6}\right)^{-1/2}\left(\frac{e}{0.1}\right), \quad (42)$$

and

$$\dot{\mu}_{\rm II} = 1.0\lambda y\delta\left(\frac{T_X}{10^6}\right)^{1/2}\left(\frac{e}{0.1}\right)\left(\frac{A}{R_\odot}\right)\left(\frac{M}{M_\odot}\right)^{-1}, \quad (43)$$

where $\gamma = (R/D)^2$, and $\delta = (A/D)^2/\beta$.

To see how the mass loss will scale with binary parameters, we calculate γ and δ assuming Roche lobe filling. These functions then depend only on the mass fraction and are shown in Figure 7. All other things being constant, we see that the mass-loss rates decrease with mass fraction and are quite small for $f < 0.1$.

We list estimated mass-loss rates for several known X-ray binary systems in Table 2. The entries for Cyg X-1 and 1700−37 are for comparison only. These systems contain massive stars which probably have radiation pressure driven mass loss exceeding the X-ray induced mass loss.

We have taken T_X to be 10^6 K for the estimates in Table 2. For gas temperatures above this, the lighter elements (C, N, and O) become ionized and their strong photoionization heating cuts off. Above 10^6 K, slower heating up to a few $\times 10^7$ K by Fe and Compton heating may occur (Kallman 1980). We estimate λ in each case from Figure 5, using the determinations of R_2 and R_3 shown in Figure 2. For case I we find that λ is quite small ($\lesssim 10^{-2}$). For case II we use a value of $\Delta = 0.1$ and find in all cases $\lambda \sim 1$. LMA calculate $P_{\rm min}$ using a more detailed treatment of the heating and cooling processes in the lower atmosphere than we have included. We adopt, from their models for HZ Her, a linear relationship between $P_{\rm min}$ and $\mathscr{L}_{X_0}$: $P_0 = 1.6 \times 10^{-12}\mathscr{L}_{x_0}$, where $P_{\rm min} = 3^{3/2}P_0$. The accretion rates needed to power the X-ray emission listed for the binaries assume $e = 0.1$, appropriate for a neutron star. For H2252−37 we also list M for $e = 0.001$, in the event that the compact star is a white dwarf.

For cases in which T_X/T_ϕ is small we are probably underestimating the mass loss, since the residual heating above 10^6 K will help the gas overcome the gravitational potential and enhance the mass-loss rate. Future work on this problem should include a more complete treatment of the heating and cooling processes of the gas at all temperatures.

A comparison of the mass-loss rates for HZ Her with those estimated by Basko *et al.* (1977) shows that our case II mass-loss rate is about the same as their maximum value. However, the physics which goes into these results is quite different. We believe that their method is in error in two ways: they include helium line cooling in estimating $P_{\rm min}$ and get a value about 10 times lower than ours, and they take the area of flow to be the whole illuminated area rather than a value some 5 times smaller, which we estimate using equation (41). Our results are about an order of magnitude larger than

ones of Alme and Wilson (1974), most likely due to a difference in the value of P_{min} by this much.

It appears from Table 2 that stars which are not close to their critical Roche lobes (for which we use case I mass-loss rates) have too small a mass-loss rate to power the X-ray emission. However, as the stars come close to filling the Roche lobe, the mass loss turns on. For the stars with $\Delta = 0.1$, we get considerable mass loss. Thus, X-ray induced winds may play a considerable role in the mass transfer of low-mass stars, but only if they have already expanded to nearly fill their Roche lobes.

We would like to thank Richard McCray and Robert Rosner for valuable discussions of this work, and Steve Hatchett for useful comments on the manuscript. This work was supported in part by the Smithsonian Institute and the National Science Foundation under grant AST 80-02404.

REFERENCES

Alme, M. L., and Wilson, J. R. 1974, *Ap. J.*, **194**, 147.
Anderson, L. 1981, *Ap. J.*, **244**, 555.
Arons, J. A. 1973, *Ap. J.*, **184**, 539.
Basko, M. M., Hatchett, S., McCray, R., and Sunyaev, R. A. 1977, *Ap. J.*, **215**, 276.
Basko, M. M., and Sunyaev, R. A. 1973, *Ap. Space Sci.*, **23**, 117.
Bradt, H. V., Doxsey, R. E., and Jernigan, J. G. 1979, *Adv. Space Exploration*, **3**, 3.
Conti, P. S. 1978, *Astr. Ap.*, **63**, 225.
Eggleton, P. P. 1971, *M.N.R.A.S.*, **151**, 351.
Holzer, T. E. 1980, in *Cool Stars, Stellar Systems, and the Sun*, ed. A. Dupree (Cambridge, Mass.: SAO Special Report 389).
Kallman, T. 1980, Ph.D. thesis, University of Colorado, Boulder.
Kippenhahn, R., Weigert, A., and Hofmeister, E. 1968, *Meth. Comput. Phys.*, **7**, 129.
London, R. 1979, Ph.D. thesis, University of Colorado, Boulder.
London, R. A., McCray, R., and Auer, L. H. 1981, *Ap. J.*, **243**, 970 (LMA).
Lubow, S. H., and Shu, F. H. 1975, *Ap. J.*, **198**, 383.
McClintock, J. E., Remillard, R. A., and Margon, B. 1981, *Ap. J.*, **243**, 900.
McCray, R., and Hatchett, S. 1975, *Ap. J.*, **199**, 196.
Parker, E. W. 1963, *Interplanetary Dynamical Processes* (New York: Wiley Interscience).
Patterson, J. P., and Jablonski, F. J. 1981, preprint.
Patterson, J. P., and Price, C. M. 1981, preprint.
Thorstenson, J., Charles, P., Bowyer, S., Briel, U. G., Doxsey, R. E., Griffiths, R. E., and Schwartz, D. A. 1979, *Ap. J. (Letters)*, **233**, L57.

RICHARD A. LONDON: Theoretical Division, L71, Lawrence Livermore Lab, P.O. Box 808, Livermore, CA 94550

BRIAN P. FLANNERY: Exxon Research and Engineering Company, Applied Math Group, P.O. Box 45, Linden, NJ 07036